An Energy-Efficient Gating Mechanism in the Acetylcholine Receptor Channel Suggested by Molecular and Brownian Dynamics

Ben Corry
Chemistry, School of Biomedical, Biomolecular and Chemical Sciences, The University of Western Australia, Crawley, WA 6009, Australia

ABSTRACT Acetylcholine receptors mediate electrical signaling between nerve and muscle by opening and closing a transmembrane ion conductive pore. Molecular and Brownian dynamics simulations are used to shed light on the location and mechanism of the channel gate. Four separate 5 ns molecular dynamics simulations are carried out on the imaged structure of the channel, a hypothetical open structure with a slightly wider pore and a mutant structure in which a central ring of hydrophobic residues is replaced by polar groups. Water is found to partially evacuate the pore during molecular simulations of the imaged structure, whereas ions face a large energy barrier and do not conduct through the channel in Brownian dynamics simulations. The pore appears to be in a closed configuration despite containing an unobstructed pathway across the membrane as a series of hydrophobic residues in the center of the channel provide an unfavorable home to water and ions. When the channel is widened slightly, water floods into the channel and ions conduct at a rate comparable to the currents measured experimentally in open channels. The pore remains permeable to ions provided the extracellular end of the pore-lining helix is restrained near the putative open configuration to mimic the presence of the ligand binding domain. Replacing some of the hydrophobic residues with polar ones decreases the barrier for ion permeation but does not result in significant currents. The channel is posited to utilize an energy efficient gating mechanism in which only minor conformational changes of the hydrophobic region of the pore are required to create macroscopic changes in conductance.

INTRODUCTION

Electrical signaling between nerve and muscle cells is controlled by the nicotinic acetylcholine receptor pore that facilitates or prevents the passage of cations into the cell. This channel has become the best characterized member of the superfamily of pentameric ligand gated ion channels that also includes gamma-aminobutyric acid, glycine, and glutamate receptors (1–3). The general shape of the protein was first determined using electron microscopy to study membrane from the *Torpedo* electric ray (4,5). This showed that the channel is formed by the symmetric arrangement of five similar but distinct subunits about a central pore. A variety of mutagenesis studies (6–9) showed that the transmembrane pore was formed by the M2 helices from each subunit, which itself is surrounded by the remaining M1, M3, and M4 helices that interact with the lipid bilayer. Since then a low resolution image of the channel in an open state (10) and two high resolution structures of the channel in a closed state (11,12) have been determined. The availability of near atomic resolution images of the channel has paved the way to tie these data together into a detailed understanding of the structural basis of receptor function.

A question of particular interest regards how the channel opens in response to the binding of acetylcholine. The low resolution electron micrograph images suggest that channel activation involves the rotation of the inner parts of the extracellular binding domain. This alters the configuration of the M2 helices, either widening or presenting polar residue to the pore (10). The conformational changes involved in channel activation have also been studied by mutations of single residues. These studies suggest that such changes take place as a wave that is initiated in the binding domain and only later passed to the transmembrane region (8,13–15).

Another contentious issue regards which region of the protein acts as the channel gate, blocking the passage of ions in the closed state. Unwin initially suggested that the gate was located midway along the M2 helix where a number of conserved hydrophobic leucine and valine residues line the pore (5,10). Mutagenesis studies reveal that this region of the pore does influence the properties of channel gating (9,16). However, the importance of this region seems to be in determining the mean open time of the channel, and mutations in each subunit appear to act independently as if these residues do not form a direct constriction that could form a gate (7,17). Substituted cysteine accessibility studies suggest the narrowest region of the channel lies at the internal end at the location of a number of charged or polar residues (residues α-240–α-244) (18,19).

Traditionally it was believed that the gating mechanism of acetylcholine receptor channel involved a physical occlusion of the pore. However, the recent high resolution image of the channel protein obtained using electron microscopy (11), and recently refined (12), shows that a continuous pathway exists through the membrane, even though the pore was imaged in a nonconducting state. This supports a hypothesis that the physical closure of the pore is not required to produce a nonconductive state (8,11,20,21). Rather, it has been suggested that a narrow pore lined by hydrophobic

Submitted June 1, 2005, and accepted for publication October 13, 2005.

Address reprint requests to Ben Corry, Tel.: 61-8-6488-3166; Fax: 61-8-6488-1005; E-mail: ben@theochem.uwa.edu.au.

0006-3495/06/02/799/12 $2.00

doi: 10.1529/biophysj.105.067868

residues can prevent the passage of ions by presenting a large dehydration barrier. Indeed, models of narrow hydrophobic pores have been shown to impede the passage of water as well as ions (20). This type of ''hydrophobic gating'' has also been suggested to be at play in the mechanosensitive channel MscS (22,23). This again raises the question as to whether the hydrophobic residues or the internal polar residues act as the channel gate.

The electrostatic properties of the channel have also been determined by measuring the reaction rates of charged reagents to cysteine mutants within the channel. These studies suggest that the electrostatic potential in the channel is significantly more positive (by ~100 mV) in the closed structure than in the open structure, which raises the possibility of an electrostatic mechanism of gating cation currents (19,24).

Since the recent electron micrograph structure of the acetylcholine receptor pore was published, there has been a huge interest in understanding how the channel gates and how ions move through the pore. This has led to a number of theoretical studies examining properties of the transmembrane structure and homology models. A Brownian dynamics (BD) study suggested that the imaged structure of the channel was nonconductive (21). Another study examined the various conformational motions of the transmembrane domain in a lipid bilayer using molecular dynamics (MD) and suggested that rapid channel gating could arise from the rotation of the side chains of the central hydrophobic residues, a process that takes place on a much faster timescale than rearrangements of the backbone (25). Although there is evidence that residues engaged in salt bridges at the intracellular end of the pore could present a physical barrier to ion conduction, MD simulations suggest that the barrier to ion permeation arises in the nonoccluded central hydrophobic region of the channel (26–28). A recent MD study of both the ligand binding and transmembrane domains of a homology model of the homomeric $\alpha 7$ protein showed a 10° rotation of part of the extracellular domain that is passed on to the transmembrane domain (29). This rotation occurs about the axis of the Cys loop and is reminiscent of the ''twist to close'' motion seen in the electron microscopy structures.

Here I examine the gating mechanism of this pore using MD and BD simulations and electrostatic calculations with the aim of shedding light on the location and mechanism of the channel gate. In particular, the experimental data supporting gating at the internal end of the pore and theoretical predictions of gating by central hydrophobic residues remain to be reconciled. The simulations described here differ from earlier studies as calculations are made on hypothetical open channel models as well as on mutant channels to see if widening the pore, or increasing hydrophilicity, can increase channel conductance. Four separate simulations are carried out on the imaged, hypothetical open, and mutant structures. In addition, BD simulations are used to relate the structures obtained from MD simulations to the channel conductance. I find that a central girdle of hydrophobic residues, rather than a physical blockage, is most likely responsible for preventing ion conduction in the closed pore by creating a large energy barrier to permeation. However, the narrowest region of the pore lies at the internal end in the closed state. The system is perfectly positioned such that only a minimal widening of the pore is required to allow ions to pass, and thus if hydrophobic gating is employed, only minimal energy is required to open or close the pore.

METHODS

Molecular dynamics simulations

To conduct MD simulations, the imaged structure of the transmembrane region of the pore (11) (Protein Data Bank (PDB) entry 1OED) is placed within a POPC lipid membrane and solvated in a flexible TIP3 water- and ion-containing box as shown in Fig. 1 *A*. The entire system contains 66,462 atoms. The trajectories of all the interacting atoms are then traced using Newton's equations of motion. Simulations are performed using NAMD (30) with a time step of 1 fs and periodic boundaries. Electrostatic interactions are calculated using the particle mesh Ewald scheme with a cutoff distance of 12 Å, whereas Lennard-Jones interactions are switched off at 10 Å. The CHARMM all atom force field parameter set (CHARMM22 for protein and CHARMM27 for lipids) is utilized. Simulations are carried out at constant pressure (1 atm) and temperature (310 K).

The lipid and water was initially energy minimized for 1000 steps and equilibrated for 10 ps with the protein held fixed. Then, harmonic constraints (3 kcal/Å^2) were applied to the α-carbon atoms of the protein, and a further 1000 steps of energy minimization and 20 ps of equilibration were performed. Finally all constraints were released and the system was energy minimized for 5,000 steps and 50 ps of simulation was conducted before data collection began. No constraints were applied to any atoms during the data acquisition runs, except for the case of the ''pinned open structure'' described below.

The volume of the hydrophobic section of the pore is required to calculate the density of water in this region during the simulation. The volume is calculated as 1.3 times the volume of an extended pentameric structure with 15 vertices determined from the coordinates of the hydrogen atom lying closest to the pore axis in each subunit for each ring of hydrophobic residues (i.e., for α-251, 255, and 259). Trajectory data were analyzed and visualized using the program VMD (31), and channel radii were calculated using the program HOLE (32).

Brownian dynamics simulations

The conductance of the channel is calculated explicitly using BD simulations. In these we trace the motions of ions in and around the channel under the influence of electric and random forces using the Langevin equation (33,34), a technique that has successfully been applied to the acetylcholine receptor (21) and other channels (35,36). The motion of individual ions is traced explicitly, but the water and protein atoms are treated as continuous dielectric media. This approximation allows simulations to be run for long enough to watch many ions pass through the pore and to examine the conductance characteristics of the channel. The channel is taken to be a rigid structure during the simulation, and partial charges are assigned to the protein using the CHARMM all atom parameter set. A number of Na^+ and Cl^- ions are placed in cylindrical reservoirs of radius 30 Å at each end of the channel that mimic the extracellular and intracellular space, and the height of the cylinder is adjusted to bring the solution to the desired concentration (150 mM). The motion of these ions under the influence of electric and random forces is then traced using the Langevin equation. The total force acting on each and every ion in the assembly is calculated and then new positions are determined for the ions a short time later. Electrostatic forces

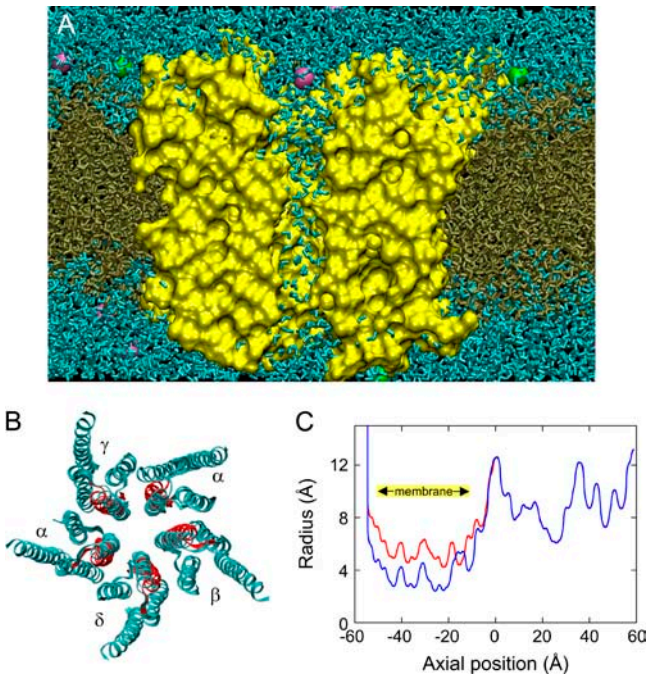

FIGURE 1 Channel structure and simulation system. (*A*) The system used for MD simulations is shown with the front half of the atoms removed to make the pore visible. The transmembrane protein (*yellow*), shown in surface representation, spans the POPC lipid membrane (*brown*) and is surrounded by water (*blue*) as well as Na^+ (*purple*) and Cl^- (*green*) ions. The entire system contains 66,462 atoms. (*B*) The transmembrane portion of the protein is comprised of five subunits each containing four membrane-spanning α-helices. The imaged structure viewed looking through the pore is shown in blue, and the putative open state structure is indicated in red. (*C*) The radius of the imaged (*blue*) and putative open (*red*) pore plotted for the transmembrane and ligand binding protein domains. The approximate axial location of the membrane is indicated by the orange bar.

are calculated by assigning dielectric constants of 2 to the protein and 60 to the water in the channel and solving Poisson's equation. A multiple time step algorithm is used, where a time step of $\Delta t = 100$ fs is employed in the reservoirs and 2 fs in the channel where the forces change more rapidly. The current is determined directly from the number of ions passing through the channel.

A grand canonical Monte Carlo scheme is used to maintain the desired ion concentrations in the reservoirs. In this, ions are created or destroyed near the edge of the reservoirs in a random manner dependent on the local electrochemical potential (37). Although the grand canonical Monte Carlo boundary conditions have been shown to produce the same results as a simpler scheme in which the total number of ions in each reservoir is kept fixed, it has an advantage when simulating a channel that holds multiple ions. A large number (~11) of ions reside in the channel and binding domain of the acetylcholine receptor at any time. Thus, when using a fixed number of ions it is difficult to set the correct number of ions on each side of the channel while allowing for some of the ions to enter the channel. The Monte Carlo scheme, on the other hand, can take account of this fact without the need for a priori knowledge of how many ions will reside in the channel and from which side they will enter. As ions enter the pore, more ions will be created in the appropriate reservoir to compensate. The membrane potential is achieved by applying a uniform field to the system and is incorporated into the solution of Poisson's equation. It should be noted that the resulting potential is far from being linear across the system, but rather drops much more rapidly in the channel than in the reservoirs. Further details of these simulations can be found elsewhere (33,34,37).

RESULTS

The acetylcholine receptor protein is part of a family of neurotransmitter gated ion channels that consist of two main functional parts: an extracellular ligand binding domain and a transmembrane pore. A representation of the transmembrane portion of the protein taken during the simulations described below and based on the imaged structure (11) is shown in Fig. 1 *A*. With the front half of the atoms removed, it can be seen that the protein (*yellow*) spans the lipid membrane (*brown*) and contains a central pathway through which ions (*spheres*) and water (*blue*) may pass. The pore is comprised of five subunits (α, β, δ, α, γ) that each contain four transmembrane helices that surround the ion conducting pathway as seen in Fig. 1 *B*. The radius of the imaged structure of the pore is plotted in blue in Fig. 1 *C* and reaches a minimum about midway through the membrane where a series of hydrophobic leucine and valine residues (α-251, α-255, α-259) form a constriction.

Here I carry out four separate 5 ns MD simulations, each with a different starting structure of the transmembrane domain embedded in a lipid bilayer and water box. The first uses the imaged structure (1OED), the second a hypothetical open structure with a wider pore described in more detail below, the third the hypothetical open structure with harmonic restraints applied to some atoms to mimic the effect of the extracellular domain, and the last a mutant version of the imaged structure in which a central ring of valine residues is replaced by polar threonine. These simulations are referred to as the ''imaged'', ''open'', ''pinned open'', and ''V255T'' models, respectively. Although the four simulations are discussed in sequence, the results are superimposed in each figure for ease of comparison.

Imaged structure

The initially solvated configuration of the imaged structure of the protein is shown in Fig. 2 *A* with the front half of the protein atoms removed to reveal the pore. The edge of the pore, where it meets the clipping plane, has been highlighted in yellow to roughly indicate the dimensions of the pore. The exact pore and protein edge are highly dependent on the orientation of the clipping plane, so readers should focus on the configuration of water in the pore rather than the dimensions of the protein, which is discussed in more detail later. It can be seen that the central region of the channel is nonpolar due to residues L-251, V-255, and V-259 on the α-subunits and the corresponding residues on the other subunits. Water molecules do not like to occupy this area and so do not form a continuous chain through the pore. When MD simulations are carried out, the pore-lining residues adjust their positions slightly and water is seen to enter the pore as illustrated in

Fig. 2 *B*, where the configuration is shown after 2.5 ns of simulation.

The root mean-square deviation (RMSD) of the backbone α-carbon atoms away from their starting position is plotted in Fig. 3 *A*. It can be seen that for this imaged structure the protein alters its configuration significantly at the start of the simulations before slowly settling down and becoming relatively stable after ~3 ns of simulation. The RMSD of the α-carbon atoms in the M2 helix is plotted in Fig. 3 *B*. This region of the protein undergoes a larger rearrangement than does the protein as a whole, suggestive of a conformational adjustment required to accommodate water within the pore. Although the M2 helix appears to be relatively stable toward the end of the simulation, some degree of fluctuation is still apparent.

In Fig. 4 *A* the density of water within the central 5 Å section of the pore, normalized by the density of bulk water (1 g/cm^3), is plotted during the 5 ns simulation. It can be seen

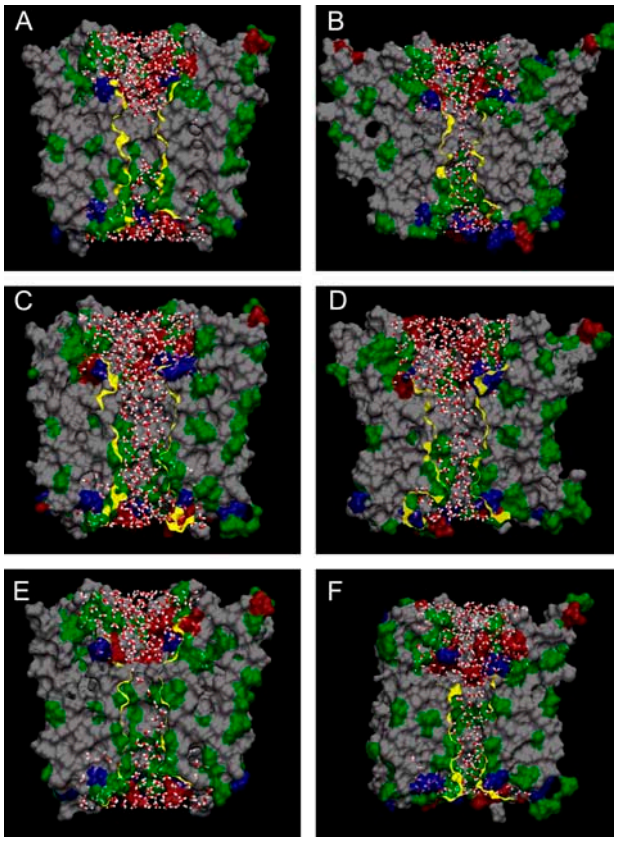

FIGURE 2 Configuration of water in the transmembrane pore during MD simulations. The positions are shown at the beginning and 2.5 ns into simulations of the imaged structure (*A* and *B*); putative open structure (*C* and *D*); and V255T mutant channel (*E* and *F*). The atomic surface of the protein is shown with the front half of the atoms removed with hydrophobic regions shown in white, polar regions in green, and acidic and basic residues shown in red and blue, respectively. To indicate the edge of the pore, the region where the protein meets the clipping plane has been highlighted in yellow. The exact shape of the pore and protein edge are highly dependent on the orientation of the clipping plane.

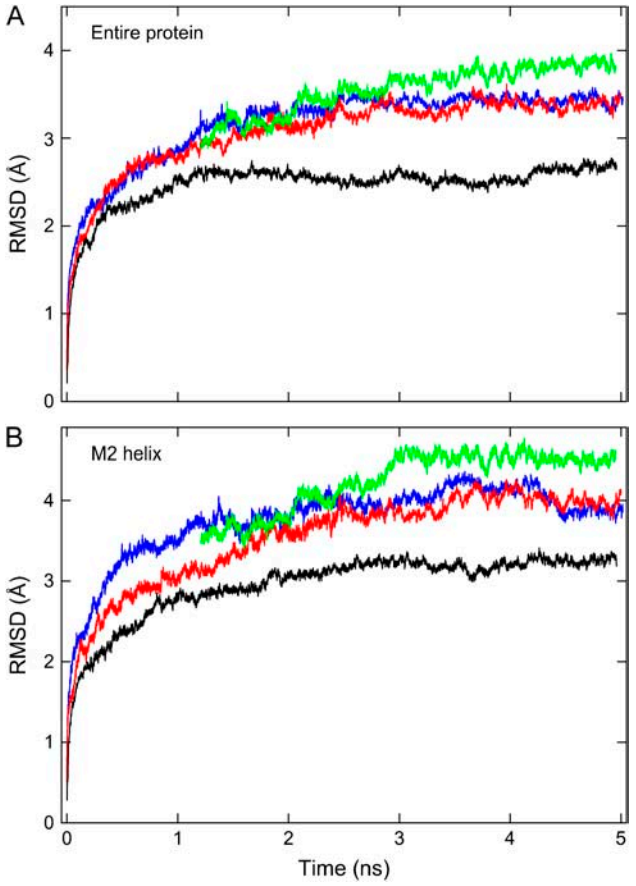

FIGURE 3 RMSD of backbone carbon atoms during MD simulations. Calculations are made for the entire protein (*A*) and M2 helix (*B*) during the simulations of the imaged (*blue*), putative open (*red*), pinned open (*black*), and V255T mutant (*green*) structures respectively.

that although water rapidly enters the pore near the start of the simulation the amount of water in the pore fluctuates considerably and the density rarely increases above 50% of its bulk value. Furthermore, twice during the simulation (~2.0 ns and ~4.3 ns) the pore becomes completely evacuated.

As suggested by Sansom and others (20) the density of water in the pore gives a good indication of the likely conductance state of the channel. In previous simulations it has been seen that if the water density is low, or the water is in a ''vapor'' state, little water will pass through the pore and ion permeation will be prevented by the desolvation barrier that must be overcome. Conversely, when the water density is above ~0.65 of the density of bulk water, water molecules do readily pass through the pore and ions can potentially permeate (20). In Fig. 4 *A* the state of the channel during the simulation is also plotted in red using this criterion. It can be seen that the channel most likely remains nonconductive to ions for the majority of the simulation. The density of water in the pore fluctuates considerably, but tends to switch between situations where zero, one, two, or three chains of water form across the hydrophobic region of the pore,

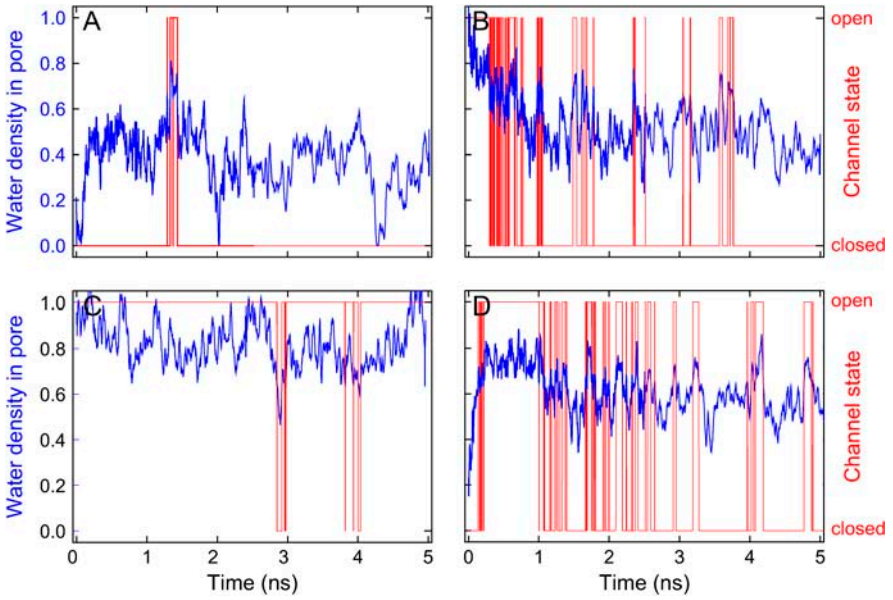

FIGURE 4 Water density and likely channel state. The density of water in the central 5 Å portion of the pore normalized by the bulk water density is plotted during MD simulations (*blue*) for the imaged pore structure (*A*); putative open structure (*B*); pinned open structure (*C*); and V255T mutant channel (*D*). The likely channel state is also shown (*red*, *right-hand scale*), assuming that the channel is closed whenever the water density in the pore falls below 0.65 times the bulk value.

corresponding roughly to densities of 0.0, 0.3, 0.5, and 0.7 times the bulk water density. Examples of the single chain configuration is shown in Fig. 2, *B* and *E*, and a double chain is shown in Fig. 2 *D*. As noted above, the channel becomes completely evacuated twice during the simulation. In addition to this, breaks in the water chains are common and ion permeation would be unlikely during these periods. Although the density of water is low in the channel, it does not remain completely empty for extended periods of many nanoseconds as was found in simulations of the MscS mechanosensitive channel (22).

The radius of the channel as calculated using the program HOLE at the start (*solid line*), middle (*dotted line*), and end (*dashed line*) of the simulation is plotted in Fig. 5 *A*. Small fluctuations in the channel radius occur throughout the simulation. The width of the hydrophobic portion of the channel, extending roughly between $z = -40$ Å and $z = -20$ Å in this figure, does not change significantly during the simulation. The largest changes in channel radius occur at each end of the channel, with the intracellular end becoming narrower and the extracellular end becoming wider. The extracellular side of the transmembrane domain would normally interact with the extracellular ligand binding domain that is absent in these simulations, so it is possible that structural changes at this end reflect the lack of nearby protein. The narrowing at the intracellular end of the protein is created by a series of charged and polar residues (residues α-240 – α-244). In particular a lysine residue on one of the α-subunits, α-242, protrudes into the pore, unlike the same residue on the other α-subunit that remains clear of the pore in a salt bridge with the glutamate residue α-241. That this intracellular end of the pore is the narrowest region is consistent with the limited accessibility of thiosulfonate groups to cysteine mutants in this region in the closed state (18,19). This lysine residue may play a role in dictating the electrostatic potential at this end of the pore. The minimum radius of the pore in each of the simulations is tabulated in Table 1.

To support the classification that the channel is nonconductive during this simulation, I calculate the energy required for an ion to pass through the channel and the likely channel conductance. To do this, I first incorporate the coordinates of the ligand binding domain (38) (PDB code 1I9B) into the transmembrane structure as described previously (21). A molecular surface is traced out as shown in Fig. 1 *C*, dielectric constants of 80, 60, and 2 are assigned to the bulk water, channel, and protein, and the energy of the ion is calculated by solving Poisson's equation using a boundary element method (39). The extracellular domain of the channel is strongly electronegative, and calculations demonstrate that it most likely holds 11 ions in stable equilibrium (21) as described in more detail below. The membrane-spanning section of the protein provides a much less favorable environment for ions. In the imaged configuration, I find that with an applied potential (−200 mV) an ion faces an energy barrier of ~19 kT centered in the hydrophobic region of the pore that it must overcome to permeate through the channel as shown in Fig. 6 *A*. At the end of the 5 ns MD simulation the barrier increases to 30 kT, confirming that the channel appears to remain in a nonconductive state.

No ions pass through either the imaged structure of the pore or the structure found at the middle or end of the 5 ns MD simulation during 5 μs of BD simulation with a −200 mV membrane potential. In Fig. 7 *A* I plot the average number of ions in layers of the channel during the BD simulation. As described above, multiple ions reside in the extracellular binding domain. Indeed, ~12 ions are found to reside in the extracellular domain and extracellular end of the transmembrane region as shown in Table 2. Notably, no ions

TABLE 1 Minimum pore radius

Model	Minimum pore radius (Å)		
	0.0 ns	2.5 ns	5.0 ns
Imaged structure	2.6	2.0	2.0
Open structure	4.0	2.4	2.6
Pinned open structure	4.0	2.4	2.2
V255T structure	2.6	2.6	2.2

The minimum pore radius is calculated using the program HOLE at the beginning (0 ns), middle (2.5 ns), and end (5.0 ns) of each MD simulation.

cross the hydrophobic region of the pore centered at $z \sim -30$ Å. The fact that no ions cross the imaged structure of the pore before or after MD simulations confirms that the channel is most likely in a nonconductive state, or at the very least the conductance is $<\sim 0.2$ pS.

The results of the BD and electrostatic calculations also give hints at the origins of valence selectivity in the channel. Cl^- ions actually face a lower energy barrier to cross the transmembrane portion of the channel than sodium ions as indicated by the dashed-dot-dot line in Fig. 6 *A*. Using the structure of the channel after either 2.5 ns or 5 ns of MD simulation (starting from the imaged structure), Cl^- ions see a barrier of ~19 kT, much less than Na^+ ions at 30 kT. However, no chloride passes through the channel during 5 μs of BD simulation. With the channel in the proposed open state discussed below, Cl^- ions do leak through the channel, with the channel favoring Na^+ at a ratio of ~6:1. When simulations are repeated using only the structure of the transmembrane portion of the protein (i.e., without the electronegative ligand binding domain) the selectivity of Na^+ ions over Cl^- is lost, with Cl^- ions being slightly favored. Thus, the transmembrane pore is not found to be selective for cations. Therefore the intra- and extracellular domains of the protein appear to be responsible for ion charge selectivity as was suggested by Unwin on inspection of the refined protein structure (12).

The conformation of the M2 helices at the start and end of the 5 ns MD simulation is illustrated in Fig. 8. In the initial imaged structure (Fig. 8 *A*) the helices are symmetrically oriented about the pore. The central ring of hydrophobic residues (V-255 on the α-subunit and equivalent residues of the other subunits, the ''V-ring'') appears to play the greatest role in decreasing the solvation of the pore as seen in previous MD simulations (25). The density of water is almost always lowest adjacent to this ring of residues, and the side chains tend to point more toward the interior of the pore than the neighboring rings of hydrophobic residues. The orientation of the side chains of the V-ring residues are also illustrated in Fig. 8. During all the simulations, this ring of residues undergoes a significant conformational rearrangement. As illustrated in Fig. 8 *B* the side chains rotate during the MD simulation such that four of the five residues can interact with the equivalent residues on the neighboring subunit. This rotation of the side chains results in an asymmetric pore shape. The backbone of the M2 helices tend to move more symmetrically, each showing a slight clockwise rotation.

Hypothetical open structure

Given that the central hydrophobic residues appear to be preventing ion conduction, I next examine the effect of widening this section of the pore. It has been shown that channel activation causes first a conformational change in the extracellular binding domain followed by a change

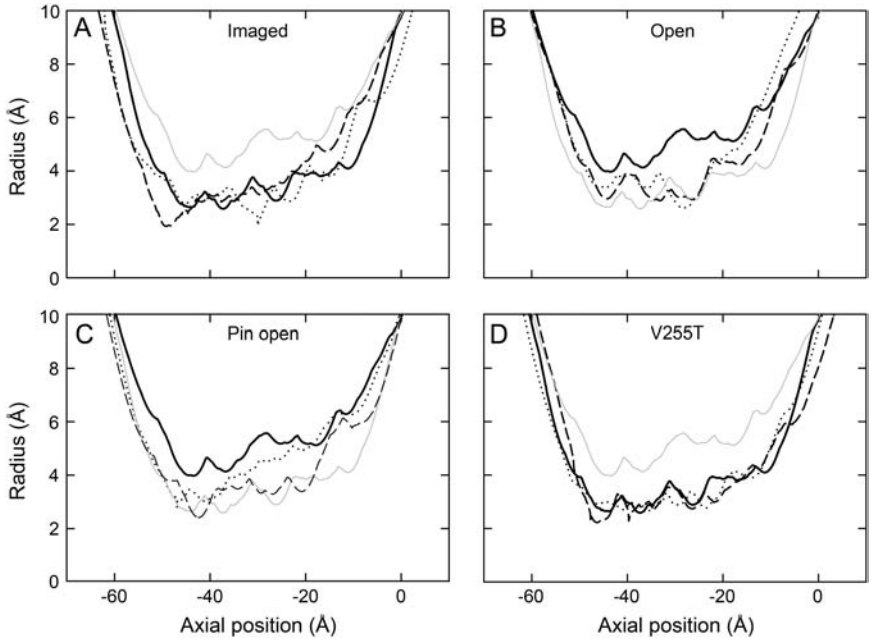

FIGURE 5 Pore radius. The radius of the pore as found using the program HOLE is plotted for the transmembrane portion of the protein at the beginning (*solid line*), middle (*dotted line*), and end (*dashed line*) of 5 ns MD simulations. Radii are plotted for the imaged structure (*A*), putative open structure (*B*), pinned open structure (*C*), and V255T mutant structure (*D*). The radius of the hypothetical open structure is also illustrated by the shaded lines in *A* and *D* for comparison, and the radii of the initial imaged structure is shown by the shaded lines in *B* and *C*.

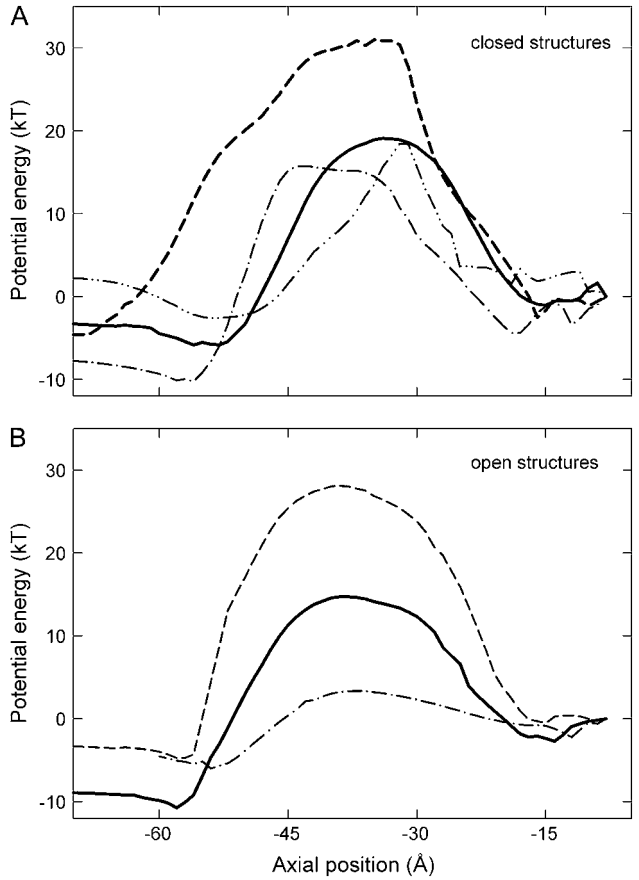

FIGURE 6 Energy barriers to ion conduction. The electrostatic potential energy is plotted for a Na^+ ion moving through the transmembrane pore, and 10 additional ions are allowed to find their minimum energy positions in the extracellular end of the pore and ligand binding domain. (*A*) The barrier is calculated for the imaged structure at the start of simulations (*solid line*); the structure after 2.5 ns of MD simulation (*dashed line*); and the V255T mutant structure after 2.5 ns of simulation (*dashed-dotted line*). Also shown is the energy barrier presented to a Cl^- ion using the imaged structure of the channel after 2.5 ns of simulation (*dashed-dotted-dotted line*). (*B*) The energy barrier to Na^+ conduction in the putative open channel at the beginning (*dashed-dotted line*) and after 2.5 ns MD simulations (*dashed line*); and the pinned open structure after 2.5 ns of simulation (*solid line*) are illustrated.

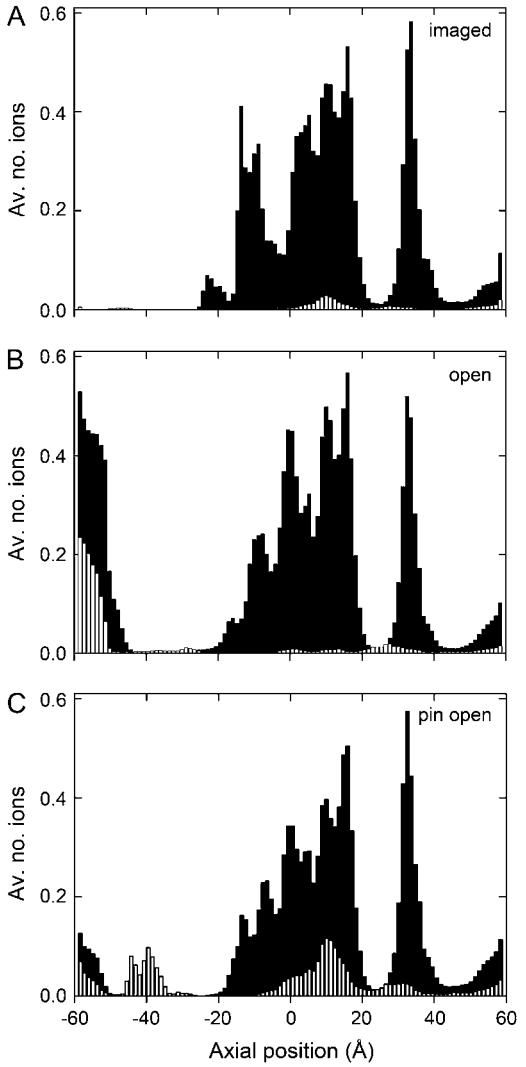

FIGURE 7 Ion dwell histogram. The locations where ions dwell in the transmembrane channel and extracellular binding domain during BD simulations are illustrated. Results are shown for Na^+ ions (*black bars*) and Cl^- ions (*white bars*) in the imaged structure (*A*), hypothetical open structure (*B*), and pinned open structure (*C*).

within the transmembrane region (40). In fact, the lower resolution electron microscope image of the open channel (10) shows a rotation of the inner β-sheets of the binding domain by 15° about the axis of the disulphide bridge joining the two β-sheets of each subunit. As the bottom of each inner sheet contacts the end of the pore-lining M2 transmembrane helix, it is suspected that this motion is transferred to the pore, and only the pore-lining M2 helix undergoes movement, whereas the rest of the transmembrane protein remains unchanged. This leaves only limited space in which the M2 helix can move, and thus limits the diameter of the open channel to be not much more than 9 Å. To replicate this open configuration, I rotate the inner M2 helix of each of the five subunits clockwise by 15° about the axis passing perpendicular to the membrane through the disulphide bridge of the binding domain as shown in red in Fig. 1 *B* and described previously (21). The intracellular end of the helix is then rotated counterclockwise by 30° to produce a slight kink as seen in the electron micrograph images (10). The net effect of this conformational change is to widen the pore by ~1.5 Å,

TABLE 2 Average number of ions in the channel and extracellular binding domain during BD simulations

Model	No. cations	No. anions
Imaged structure	12.1	0.3
Open structure start	11.7	0.4
Open structure end	12.1	0.2
Pinned open structure	10.9	2.0
V255T structure	11.1	1.3

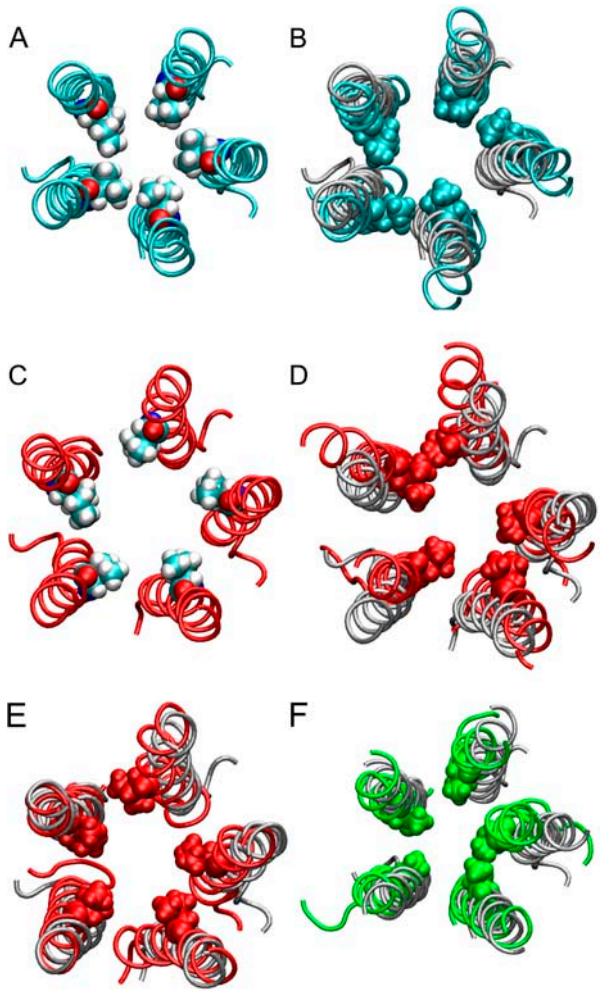

FIGURE 8 Conformations of the M2 helices. The conformation of the M2 helices as well as the side chains of the central hydrophobic residue (VAL255 in the α-subunit and equivalent residues on the other subunits) are illustrated at the beginning (*A*) and end (*B*) of the simulation of the imaged structure; the beginning (*C*) and end (*D*) of the simulation of the putative open structure; the end of the simulation of the pinned open structure (*E*) and the end of the simulation of the V255T mutant structure (*F*). The configuration of the M2 helix at the start of each simulation is indicated by the gray tubes.

with the minimum radius increasing from 2.6 to 4.0 Å as indicated in Fig. 1 *C* and Table 1.

MD simulations are carried out with the pore in this putative open state. The initial and final configurations of the protein and water in the pore are shown in Fig. 2, *C* and *D*. It is clear that water readily floods into the channel at the start of the simulation; however, by the end the amount of water in the pore is considerably less. The RMSD fluctuation of the protein is illustrated in Fig. 3. The protein appears relatively stable, although the M2 helix still shows some degree of fluctuation at the end of the simulation.

As shown in Fig. 4 *B* water readily enters the widened channel and occupies it at close to the bulk density. In the initial configuration, electrostatic calculations indicate that under an applied potential Na^+ ions have only to overcome a 3.4 kT energy barrier to conduct through the channel (Fig. 6 *B*). Indeed, ions are seen to pass readily through the channel during BD simulations at a conductance of ~22 pS, close to the experimentally measured result in which the channel has been shown to have conductance substates of 15, 25, and 35 pS (41). The locations where ions dwell during the BD simulations of this hypothetical open state are plotted in Fig. 7 *B*. Although the positions of ions in the extracellular domain look very similar to those seen for the imaged structure, there is now a very small number of ions in the hydrophobic region of the channel created by the passage of ions. It is worth noting that the same hydrophobic residues line the pore in both the closed and starting open structures described above. This suggests that it is the widening of the pore that is important for allowing water and ions to enter this model channel, not specific motions of the M2 helices or the presentation of different residues to the pore.

During a 5 ns MD simulation, it can be seen from Fig. 4 *B* that water slowly evacuates the pore and it returns to a configuration close to the imaged state of the pore. The water density decreases to below 0.5 of its bulk value (Fig. 4 *B*), the minimum radius of the pore shrinks to 2.4 Å (Table 1), the energy barrier to conduction increases to 28 kT (Fig. 6 *B*), and the conductance of the channel drops to zero in BD (Table 3), all of which suggests that the channel has returned to a closed state. An examination of the pore radius shown in Fig. 5 *B* indicates that not only has the overall radius of the pore decreased, but that the central hydrophobic region now represents the narrowest portion of the channel. Indeed the channel radius at the end of 5 ns of simulation is remarkably similar to the radius of the imaged structure in the middle of the simulation.

It is not surprising that the protein appears to return to a closed state during the MD simulation, as it is carried out in

TABLE 3 Energy barriers and currents for various channel structures

Situation	Potential energy barrier (kT)	Current (pA)
Imaged structure	19.1	0.0
Imaged + 2.5 ns simulation	30.9	0.0
Open structure + energy minimization	3.4	4.4 ± 0.3
Open structure + 2.5 ns simulation	28.1	0.03 ± 0.03
V255T mutant + 2.5 ns simulation	15.7	0.2 ± 0.1
Pin open + 2.5 ns simulation	14.7	2.0 ± 0.4
Imaged + 2.5 ns simulation, Cl^- ion	19.0	0.0

Potential energy barriers for a Na^+ ion to cross the transmembrane region of the pore are calculated using Poisson's equation with 10 other Na^+ ions resident in the extracellular domain. The last row represents the energy barrier seen by a Cl^- ion with 11 Na^+ ions in the extracellular domain. Each current value is calculated from a 5 μs BD simulation. All calculations made with a −200 mV membrane potential.

the absence of the extracellular ligand binding domain. Not only does this extracellular domain initiate the opening of the channel, it is likely to hold the channel in its open state. Without this, there is nothing keeping the channel open and it would be likely to relax to a nonconductive state. Surprisingly, the RMSD of the open channel simulation is not significantly larger than that obtained for the imaged structure, despite the fact that the channel appears to close to a nonconductive state during this simulation.

During the simulation, the M2 helices rotate counterclockwise roughly about the axis of the disulphide bridge in the extracellular domain, back toward the imaged state of the channel, and also gain a larger kink in the middle of the pore as depicted in Fig. 8 *D*. As with the simulation of the imaged structure, the side chains of the residues in the V-ring rotate in an asymmetric manner such that four of the five residues can interact in pairs.

Pinned open structure

To examine whether the lack of the extracellular domain is responsible for the apparent channel closure in the simulation of the hypothetical open structure, an additional simulation is carried out in which the extracellular end of the transmembrane M2 helices are held near their initial positions. To do this, the α-carbons of three residues at the extracellular end of the M2 helix where it is likely to interact with the extracellular binding domain (residues 270–272 on the α-subunit and equivalent residues on the other subunits) are held with harmonic restraints of 5 kcal/Å^2, whereas no constraints are applied to the remainder of the system. MD simulations are conducted to see if this channel configuration remains in a conductive state. Due to the restraints, this simulation is considerably more stable than any of the others as evident in the RMSD plotted by the black lines in Fig. 3. Both the protein as a whole and the M2 helices remain much closer to their starting position than in the previous simulations.

The starting structure is the same as that for the hypothetical open structure and so the pore is filled with water and conducts in BD simulations. The water density in the pore during the simulation is plotted in Fig. 4 *C*. It is clear that water remains in the pore at close to its bulk density for the entirety of the simulation. The state analysis based on the water occupancy suggests that the pore remains in the conductive state for the majority of the simulation, suggesting that if the ends of the M2 helices are held in the open configuration by the extracellular domain, then the channel will remain in the conductive state. Surprisingly, an analysis of the pore radii indicates that the minimum radius of the pore decreases from 4.0 Å to 2.4 Å during the course of the simulation, a similar decrease to that seen in the simulation without restraints. A question arises, therefore, as to why the pore maintains a high density of water during this simulation, but not in the unconstrained simulation. An examination of the pore radius plotted in Fig. 5 *C* indicates that although the pore narrows considerably, this narrowing occurs predominantly at the intracellular end of the channel where the protein is polar. The radius at the hydrophobic girdle is considerably larger in this simulation than at the end of the unconstrained simulation or during the simulation of the imaged structure. This supports the conclusion that it is the width of the hydrophobic region of the pore that is crucial for determining whether water or ions will pass through the channel.

Despite remaining solvated for the duration of the MD simulation, electrostatic calculations on the final structure indicate that ions face a considerable energy barrier, of over 14 kT, to cross the channel as shown in Fig. 6 *B*. However, when BD simulations are carried out using the final structure, ions are found to permeate through the channel at a conductance of ~10 ps. It is somewhat surprising that ions are able to overcome this energy barrier and conduct at the rate observed, but a closer inspection of the BD simulations reveals how this arises. First, the fact that multiple Na^+ ions reside at the extracellular end of the channel means that the thermal energy of many ions can aid the ion crossing the hydrophobic region of the pore as the fluctuations in ion positions can become correlated. More importantly, however, an analysis of the number of ions in the pore indicates that two anions also occupy the channel as seen in Fig. 7 *C* and Table 2. These anions will undoubtedly aid the passage of cations through the pore. In particular, about half the time an anion is located near the extracellular end of the channel where its attractive potential can assist cations in permeating the hydrophobic center of the pore.

As pictured in Fig. 8 *E*, the M2 helices of the pinned open structure undergo much smaller changes during the MD simulations than in the unconstrained simulation. Because the top of the helix is restrained it cannot undergo the counterclockwise rotation toward the imaged structure. The main motion of the helix is an increased kink caused by motion of its intracellular end. Importantly, the protein maintains its symmetrical structure with neither residues in the V-ring or ''L-ring'' able to directly interact in pairs as seen previously. It has been suggested that opening the channel involves breaking the ''hydrophobic'' interactions between these rings of residues (10). This simulation lends plausibility to this hypothesis. If the hydrophobic rings can be kept in a symmetrical noninteracting arrangement, then this keeps the center of the channel open and allows for water or ion conduction.

The conformational changes seen during the MD simulation of the hypothesized open structures possibly represent the type of motion involved in channel gating. For this reason it is of interest to investigate the energy involved in this conformational shift to ascertain the feasibility of this rearrangement. The total energy of the system decreases significantly during all the MD simulations as shown in Fig. 9. The difference between the energy drops in the simulations of the unconstrained open, pinned open, and imaged conformations from the start of the dynamic simulation and the

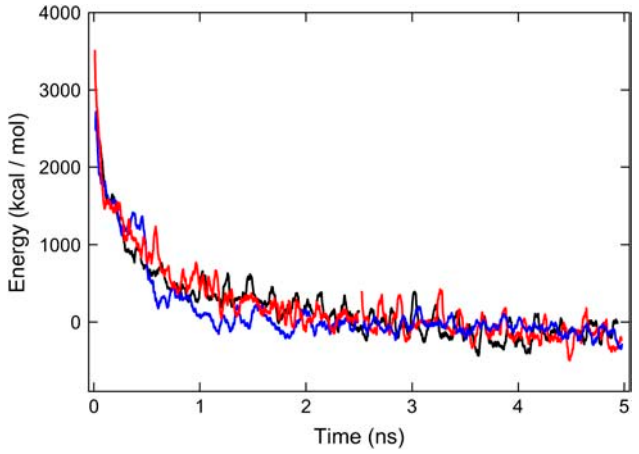

FIGURE 9 Total energy of the system during MD simulations. The total energy is plotted for the simulation of the imaged (*blue*), putative open (*red*), and pinned open (*black*) structures, sampling the energy every pS. Average energy values, in which the data is averaged in a moving 25 pS window, are shown.

end are minimal, as is clear in the moving average of the energy that is plotted. As the total energy of the system fluctuates significantly it is difficult to estimate accurate energy differences, although the difference between the closed and open state is within 100 kcal/mol. It has been estimated from the binding energy of acetylcholine that the energy available to induce the conformational change involved in channel opening is only ~10 kcal/mol and must at most be <30 kcal/mol (42). Although only a crude estimate, the minimal energy difference seen between the putative open and closed states in this study is consistent with these figures.

V255T mutant structure

Given that a widening of the pore is able to dramatically increase the water occupancy and conductance of the channel, it is of interest to see if making the central region of the pore more hydrophilic can have the same effect. To do this I replace 5 of the 15 central hydrophobic residues comprising the V-ring (residues 255, 261, 269, and 264 in the α-, β-, γ-, and δ-subunits) with polar threonine in the imaged structure.

The RMSD plots for a 5 ns MD simulation (*green lines*, Fig. 3) show this to be the least stable of all the simulations, with deviations away from the starting point continuing for the entire 5 ns. Presumably the sudden change in the chemical nature of the pore has a large influence on its conformation. Although longer simulations would be appreciated for this configuration, some trends in the behavior of this mutant in comparison with the behavior of the other models are still apparent.

This mutation can be seen to disrupt the closed state of the pore. Few water molecules reside in the channel at the start of the simulation (Fig. 2 *E*), but water rapidly enters as seen in Fig. 2 *F*. Indeed a plot of the water density in the pore (Fig. 4 *D*) indicates that water occupies the channel at a density of ~0.6 times the bulk value for the majority of the simulation. The state analysis of the water density shows that the pore rapidly fluctuates between open and closed, suggesting that it is at a critical midpoint between conducting and nonconducting states, although it spends the majority of the later half of the simulation in a closed state.

Despite having the largest RMSD, the radius of the pore shows the least change during MD simulations as illustrated in Fig. 5 *D*. The pore profile is very similar at the beginning, middle, and end of the simulation. The intracellular end of the pore again becomes the narrowest point in the channel.

Electrostatic calculations employing the final configuration from the MD simulations find an energy barrier of 16 kT to Na^+ conduction as illustrated in Fig. 6 *A*. The conductance during BD simulations is low at only 0.2 pS. Although the energy barrier to cation conduction is similar to that seen in the pinned open structure, anions do not appear to occupy this channel to aid in ion conduction. The low conductance in the mutant channel is consistent with experiments in which a hydrophobic residue from a neighboring ring (α-251) has been replaced by a polar one (7,17). These found that the rate of channel closure was decreased and the sensitivity to acetylcholine was increased. This suggests that such mutations disrupt the channel gate to favor the open state. By themselves, however, these mutations are not enough to make the channel conduct significantly in its closed state. The effect of these mutations on the conductance of the open channel remains to be determined.

The picture of the M2 helices shown in Fig. 8 *F* indicates that these helices move inward in a symmetric manner during the simulation. This would be expected to decrease the radius in the center of the channel, although this is not obvious in the pore radii profile plotted in Fig. 5 *D*. The ring of mutated residues maintains a more symmetrical arrangement than in the wild-type protein which may help to keep the radius of this region of the pore larger than would be expected from the position of the backbone.

DISCUSSION

Numerous lines of evidence presented in this work suggest that the imaged structure of the acetylcholine receptor channel is in a closed state. The channel remains only partially solvated during MD simulations, the energy barriers to ion permeation found from electrostatic calculations are large, and no current is found to pass through the channel in BD simulations. Furthermore, as the channel does not contain a physical blockage, and given the location of the energy barrier to ion permeation, it is apparent that it is the hydrophobic nature of the central pore-lining residues that prevents ion conduction by providing an unfavorable home for water and a desolvation barrier to ions.

Simulations in simplified pore models have previously shown that such hydrophobic residues provide a very efficient gating mechanism, as only very minor changes in channel

radius or hydrophobicity are required to have a major influence on the chance of ion permeation (20,43,44). These studies showed that there was a critical radius of ~5 Å for the model pore studied, above which the state of a hydrophobic channel changes from closed to open, presumably as enough water molecules can then enter the channel to form a self-hydrating hydrogen bonding network. Here it is demonstrated that this ''hydrophobic gating'' effect could be at play in the acetylcholine receptor pore. The imaged structure has a hydrophobic region whose radius of just under 3 Å lies below this critical value. When the radius is increased above 4 Å the channel becomes highly conductive. The critical radius found in this study of the acetylcholine receptor is less than was found in the model pores, possibly because the hydrophobic region is surrounded by a number of polar residues. It is worth noting that although the central hydrophobic residues appear to be responsible for preventing ion conduction, the narrowest region of the channel appears to be farther to the intracellular end.

Although the hypothetical open structure presented in this study is based on experimental data, there is not enough information to determine the accuracy of this model. However, it is important to note that the main conclusion of this study, the fact that the acetylcholine receptor pore can be made highly conductive by a slight widening of the hydrophobic region of the pore, does not rely on the accuracy of the open structure presented. If the putative open structure is close to the actual open state of the acetylcholine receptor pore, then this study also emphasizes the importance of the extracellular domain in holding the channel in its open state. Without the presence of this domain, the transmembrane pore relaxes to a nonconductive configuration. Presumably the presence of acetylcholine is required to maintain the protein in its conductive conformation.

Surprisingly, a reduction of the hydrophobicity of the pore was not of itself enough to make the imaged structure of the pore conductive to ions. Although replacing the hydrophobic V-ring with polar residues decreased the energy barrier to ion conduction, the greatest effect of this mutation may be to destabilize the interaction among residues within this ring. Replacing the van der Waals interactions between the side chains with interactions with water in the pore may assist the separation of these residues required to open the channel.

The 5 ns MD simulations presented here are not long enough to witness large scale conformational changes away from the starting structures. However some important motions, including the symmetric motion of the M2 helices and the asymmetric rotation of the hydrophobic side chains, can be seen. More importantly some clear trends in water occupancy and barriers to ion permeation are visible despite the length of the simulations. For example, the low density in the simulation of the imaged structure, the high density in the putative open structure, and the differences between the open and pinned open structure are unlikely to be affected by the simulation length.

The results of this study lend plausibility to the concept that a hydrophobic region of the pore acts as the channel gate in the acetylcholine receptor; however, other mechanisms still cannot be ruled out. The hydrophobic gating mechanism proposed provides a very energy efficient way to control ion flow, as only minor conformational changes are required to open the pore. Creating physical blockages, on the other hand, would probably require larger structural rearrangements. In addition, opening an occluded pore requires the separation of attractive regions of the protein, which may involve breaking electrostatic bonds rather than just van der Waals interactions. Using the hydrophobic gating mechanism, a small amount of energy creating a minimal microscopic change can cause major macroscopic effects.

This research was supported by funding from the Australian Research Council and some calculations were carried out at the National Facility of the Australian Partnership for Advanced Computing.

REFERENCES

1. Karlin, A., and M. H. Akabas. 1995. Toward a structural basis for the function of nicotinic acetylcholine receptors and their cousins. *Neuron.* 15:1231–1244.
2. Karlin, A. 2002. Emerging structure of the nicotinic acetylcholine receptors. *Nat. Rev. Neurosci.* 3:102–114.
3. Absalom, N. L., T. M. Lewis, and P. R. Scholfield. 2004. Mechanisms of channel gating of the ligand-gated ion channel superfamily inferred from protein structure. *Exp. Physiol.* 89:145–153.
4. Toyoshima, C., and N. Unwin. 1990. Three-dimensional structure of the acetylcholine receptor by cryoelectron microscopy and helical image reconstruction. *J. Cell Biol.* 111:2623–2635.
5. Unwin, N. 1993. Nicotinic acetylcholine receptor at 9 Å resolution. *J. Mol. Biol.* 229:1101–1124.
6. Changeux, J. P., J. I. Galzi, A. Devillers-Thiry, and D. Bertrand. 1992. The functional architecture of the acetylcholine nicotinic receptor explored by affinity labelling and site-directed mutagenesis. *Q. Rev. Biophys.* 25:395–432.
7. Labarca, C., M. W. Nowak, H. Zhang, L. Tang, P. Deshpande, and H. A. Lester. 1995. Channel gating governed symmetrically by conserved leucine residues in the M2 domain of nicotinic receptors. *Nature.* 376:514–516.
8. Corringer, P. J., N. Le Novere, and J. P. Changeux. 2000. Nicotinic receptors at the amino acid level. *Annu. Rev. Pharmacol. Toxicol.* 40:431–458.
9. Lester, H. 1992. The permeation pathway of neurotransmitter-gated ion channels. *Annu. Rev. Biophys. Biomol. Struct.* 21:267–292.
10. Unwin, N. 1995. Acetylcholine receptor channel imaged in the open state. *Nature.* 373:37–43.
11. Miyazawa, A., Y. Fujiyoshi, and N. Unwin. 2003. Structure and gating mechanism of the acetylcholine receptor pore. *Nature.* 423:949–955.
12. Unwin, N. 2005. Refined structure of the nicotinic acetylcholine receptor at 4 Å resolution. *J. Mol. Biol.* 346:967–989.
13. Lester, H. A., M. I. Dibas, D. S. Dahan, J. F. Leite, and D. A. Dougherty. 2004. Cys-loop receptors: new twists and turns. *Trends Neurosci.* 27:329–336.
14. Grosman, C., M. Zhou, and A. Auerbach. 2000. Mapping the conformational wave of acetylcholine receptor channel gating. *Nature.* 403:773–776.
15. Cymes, G. D., C. Grosman, and A. Auerbach. 2002. Structure of the transition state of gating in the acetylcholine receptor channel pore: a phi-value analysis. *Biochemistry.* 41:5548–5555.

16. Bertrand, D., J. L. Galzi, A. Devillers-Thiéry, S. Bertrand, and J. P. Changeux. 1993. Stratification of the channel domain in neurotransmitter receptors. *Curr. Opin. Cell Biol.* 5:688–693.

17. Filatov, G. N., and M. M. White. 1995. The role of conserved leucines in the M2 domain of the acetylcholine receptor in channel gating. *Mol. Pharmacol.* 48:379–384.

18. Wilson, G. G., and A. Karlin. 1998. The location of the gate in the acetylcholine receptor channel. *Neuron.* 20:1269–1281.

19. Pascual, J. M., and A. Karlin. 1998. State-dependent accessibility and electrostatic potential in the channel of the acetylcholine receptor: inferences from rates of reaction of thiosulfonates with substituted cysteines in the M2 segment of the alpha subunit. *J. Gen. Physiol.* 111:717–739.

20. Beckstein, O., and M. S. P. Sansom. 2004. The influence of geometry, surface character, and flexibility on the permeation of ions through biological pores. *Phys. Biol.* 1:42–52.

21. Corry, B. 2004. Theoretical conformation of the closed and open states of the acetylcholine receptor channel. *Biochim. Biophys. Acta.* 1663: 2–5.

22. Anishkin, A., and S. Sukharev. 2004. Water dynamics and dewetting transitions in the small mechanosensitive channel MscS. *Biophys. J.* 86:2883–2895.

23. Sotomayor, M., and K. Schulten. 2004. Molecular dynamics study of gating in the mechanosensitive channel of small conductance MscS. *Biophys. J.* 87:3050–3065.

24. Wilson, G. G., J. M. Pascual, N. Brooijmans, D. Murray, and A. Karlin. 2000. The intrinsic electrostatic potential and the intermediate ring of charge in the acetylcholine receptor channel. *J. Gen. Physiol.* 115:93–106.

25. Xu, Y., F. J. Barrantes, X. Luo, K. Chen, J. Shen, and H. Jiang. 2005. Conformational dynamics of the nicotinic acetylcholine receptor channel: a 35-ns molecular dynamics simulation study. *J. Am. Chem. Soc.* 127: 1291–1299.

26. Saiz, L., and M. L. Klein. 2005. The transmembrane domain of the acetylcholine receptor: insights from simulations and synthetic peptide models. *Biophys. J.* 88:959–970.

27. Saladino, A. C., Y. Xu, and P. Tang. 2005. Homology modeling and molecular dynamics simulations of transmembrane domain structure of human neuronal nicotinic acetylcholine receptor. *Biophys. J.* 88:1009–1017.

28. Hung, A., K. Tai, and M. S. P. Sansom. 2005. Molecular dynamics simulation of the M2 helices within the nicotinic acetylcholine receptor transmembrane domain: structure and collective motions. *Biophys. J.* 88:3321–3333.

29. Law, R. J., R. H. Henchman, and J. A. McCammon. 2005. A gating mechanism proposed from a simulation of a human 7 nicotinic acetylcholine receptor. *Proc. Natl. Acad. Sci. USA.* 102:6813–6818.

30. Kalé, L., R. Skeel, M. Bhandarkar, R. Brunner, A. Gursoy, N. Krawetz, J. Phillips, A. Shinozaki, K. Varadarajan, and K. Schulten. 1999. NAMD2: greater scalability for parallel molecular dynamics. *J. Comp. Phys.* 151:283–312.

31. Humphrey, W., A. Dalke, and K. Schulten. 1996. VMD: visual molecular dynamics. *J. Mol. Graph.* 14:33–38.

32. Smart, O. S., J. G. Neduvelil, X. Wang, B. A. Wallace, and M. S. P. Sansom. 1996. Hole: a program for the analysis of the pore dimensions of ion channel structural models. *J. Mol. Graph.* 14:354–360.

33. Li, S. C., M. Hoyles, S. Kuyucak, and S. H. Chung. 1998. Brownian dynamics study of ion transport in the vestibule of membrane channels. *Biophys. J.* 74:37–47.

34. Chung, S. H., T. W. Allen, and S. Kuyucak. 2002. Conducting state properties of the KcsA potassium channel from molecular and Brownian dynamics simulations. *Biophys. J.* 82:628–645.

35. Corry, B., T. W. Allen, S. Kuyucak, and S. H. Chung. 2001. Mechanisms of permeation and selectivity in calcium channels. *Biophys. J.* 80:195–214.

36. Allen, T. W., and S. H. Chung. 2001. Brownian dynamics study of an open-state KcsA potassium channel. *Biochim. Biophys. Acta.* 1515: 83–91.

37. Corry, B., M. Hoyles, T. W. Allen, M. Walker, S. Kuyucak, and S. H. Chung. 2002. reservoir boundaries in Brownian dynamics simulations of ion channels. *Biophys. J.* 82:1975–1982.

38. Brejc, K., W. J. van Dijk, R. V. Klaassen, M. Schuurmans, J. van Der Oost, A. B. Smit, T. K. Sixma. 2001. Crystal structure of an Ach-binding protein reveals the ligand binding domain of nicotinic receptors. *Nature.* 411:269–276.

39. Hoyles, M., S. Kuyucak, and S. H. Chung. 1998. Computer simulation of ion conductance in membrane channels. *Phys. Rev. E.* 58:3654–3661.

40. Grosman, C. 2002. Linear free-energy relationships and the dynamics of gating in the acetylcholine receptor channel: a phi-value analysis of an allosteric transition at the single-molecule level. *J. Biol. Phys.* 28:267–277.

41. Hamill, O. P., and B. Sakmann. 1981. Multiple conductance states of single acetylcholine receptor channels in embryonic muscle cells. *Nature.* 294:462–464.

42. Jackson, M. B. 1982. Perfection of a synaptic receptor: kinetics and energetics of the acetylcholine receptor. *Proc. Natl. Acad. Sci. USA.* 86:2199–2203.

43. Beckstein, O., P. C. Biggin, and M. S. P. Sansom. 2001. A hydrophobic gating mechanism for nanopores. *J. Phys. Chem. B.* 105:12902–12905.

44. Beckstein, O., and M. S. P. Sansom. 2003. Liquid-vapor oscillations of water in hydrophobic nanopores. *Proc. Natl. Acad. Sci. USA.* 100: 7063–7068.